Structure, Vol. 11, 1513–1520, December, 2003, ©2003 Elsevier Science Ltd. All rights reserved. DOI 10.1016/j.str.2003.11.009

The Crystal Structures of EDA-A1 and EDA-A2: Splice Variants with Distinct Receptor Specificity

Sarah G. Hymowitz,[1,*] Deanne M. Compaan,[1] Minhong Yan,[2] Heidi J.A. Wallweber,[1] Vishva M. Dixit,[2] Melissa A. Starovasnik,[1] and Abraham M. de Vos[1]

[1]Department of Protein Engineering

[2]Department of Molecular Oncology

Genentech, Inc.

1 DNA Way

South San Francisco, California 94080

Summary

EDA is a tumor necrosis factor family member involved in ectodermal development. Splice variants EDA-A1 and EDA-A2 differ only by the presence of Glu 308 and Val 309 in the expected receptor binding region of EDA-A1 but not EDA-A2. This two amino acid difference functions as a switch controlling receptor specificity. EDA-A1 binds only to EDAR, while EDA-A2 is specific for XEDAR. In order to understand the structural basis of this switch, we determined the X-ray crystal structures of the TNF domain of both EDA-A1 and EDA-A2 at 2.3 Å and 2.2 Å, respectively. While the backbone conformation around the splice difference is similar in both isoforms, the conformation of the following loop, the surface charge, and the shape of the expected receptor binding site differ significantly.

Introduction

The TNF families of ligands (TNFLs) and receptors (TNFRs) influence a variety of biological pathways, including immune system regulation, apoptosis, and inflammation (Locksley et al., 2001). The distantly related TNFL protein ectodysplasin (EDA) is involved in ectodermal development (Srivastava et al., 1997; Monreal et al., 1998; Bayés et al., 1998; Tucker et al., 2000; Laurikkala et al., 2002; Mikkola and Thesleff, 2003). Like other TNFL family members, EDA is a type II transmembrane protein with a C-terminal TNF domain. EDA also contains several other structural features, including a furin site and a collagen-like sequence in the linker region between the transmembrane helix and the TNF domain (Schneider et al., 2001; Wisniewski et al., 2002). The EDA gene transcript is present in several splice forms (Srivastava et al., 1997; Monreal et al., 1998; Bayés et al., 1998). Two of these splice forms contain all of the described features, differing only by a two amino acid motif, Glu 308 and Val 309, which is present in EDA-A1 but not in EDA-A2 (Bayés et al., 1998; Yan et al., 2000). Interestingly, this difference is sufficient to confer absolute receptor specificity. EDA-A1 binds EDAR, a member of the TNFR family involved in ectodermal development, while EDA-A2 binds to the related receptor, XEDAR (Bayés et al., 1998; Yan et al., 2000), which shares only 22% sequence identity with EDAR in their extracellular regions. Unlike some subgroups of the TNFL family, such as BAFF and APRIL, LT and TNF, or FasL, LIGHT, and TL1A (Bodmer et al., 2002; Migone et al., 2002), in which either the ligands or the receptors are promiscuous, EDA-A1 and EDA-A2 are thus far known to interact only with EDAR and XEDAR, respectively.

The intracellular domains and signaling pathways of EDAR and XEDAR are also divergent, amplifying the switch between EDA-A1 and EDA-A2. EDAR possesses an intracellular death domain which interacts with the adaptor EDARDD, which in turn interacts with TRAFs 1, 2, and 3 (Headon et al., 2001; Yan et al., 2002). XEDAR lacks a death domain and has been shown to signal via TRAF-6 (Yan et al., 2000; Naito et al., 2002; Sinha et al., 2002). Specific mutations in EDA, EDAR, EDARDD, and TRAF6 result in symptoms of hypohidrotic ectodermal dysplasia (HED), which is characterized by defects in sweat glands, hair follicles, and teeth (Monreal et al., 1998; Tucker et al., 2000; Headon et al., 2001; Naito et al., 2002). The biology of the EDA-A2/XEDAR pathway is not as well characterized as that of EDA-A1/EDAR.

Although EDA is one of the most divergent TNFLs, both XEDAR and EDAR are conventional TNFRs with three cysteine-rich pseudorepeats (CRDs) in their extracellular domains. Both receptors are missing the last of the three canonical disulfide bridges in CRD3, and EDAR is missing an additional disulfide bridge in CRD2. However, the remaining protein sequence of both EDAR and XEDAR suggests that they are representative members of the TNFR family with structural similarity to TNFR1. Thus, each is expected to bind its cognate ligand in a fashion similar to that seen in the crystal structures of the LT/TNFR1 (Banner et al., 1993) and Apo2L (TRAIL)/DR5 (Hymowitz et al., 1999; Mongkolsapaya et al., 1999; Cha et al., 2000) complexes, in which the receptors make contacts along the monomer-monomer interfaces of the ligand. In particular, two CRDs from the receptor are expected to contact ligand, with one of these domains mediating contacts to the surface of the ligand in the vicinity of the alternative splicing receptor specificity "switch."

In order to better understand the relationship of EDA to other TNFLs, as well as how the two amino acid "switch" between EDA-A1 and EDA-A2 controls specificity for their respective receptors, we have determined the structure of the TNF domains of EDA-A1 and EDA-A2. These structures show that the two amino acid difference between EDA-A1 and A2 dramatically influences the shape and charge of approximately half of the expected receptor binding interface. Interestingly, some of the HED missense mutations in the TNF domain of EDA are located in this region and thus might directly influence receptor binding.

Results and Discussion

Overall Structure of EDA-A1 and EDA-A2

The 2.3 Å crystal structure of a fragment of EDA-A1 containing residues 233–391 was solved by molecular

*Correspondence: hymowitz@gene.com

Table 1. Data Collection and Refinement Statistics

	EDA-A1	EDA-A2
Data Collection		
Resolution (Å)	30–2.30 (2.38–2.30)[a]	30–2.23 (2.40–2.23)[a]
R_{sym}[b]	0.081 (0.239)[a]	0.03 (0.079)[a]
Space group	$P2_1$	$P2_1$
Unit cell (Å)	a = 53.6, b = 298, c = 54.3	a = 50.7, b =161, c = 51.0
(°)	β = 91.4	β = 105
Number of observations	215,586	101,523
Unique reflections	66,596	37,259
Completeness (%)	94.4 (93.1)[a]	96.8 (93.1)[a]
Refinement		
Resolution (Å)	20–2.30	30–2.23
Number of reflections	66,278	37,223
Final R[c], R_{free} (F > 0)	0.195, 0.261	0.200, 0.241
Number of residues	1731	840
Number of solvent molecules	339	182
Number of non-H atoms	13896	6776
Rmsd bonds (Å)	0.010	0.007
Rmsd angles (°)	1.28	1.16
Rmsd B (bonded atoms) (Å^2)	1.9	1.6

[a] Numbers in parentheses refer to the highest resolution shell.
[b] $R_{sym} = \Sigma|I - \langle I\rangle|/\Sigma I$. $\langle I\rangle$ is the average intensity of symmetry related observations of a unique reflection.
[c] $R = \Sigma|F_o - F_c|/\Sigma F_o$. R_{free} is calculated as R, but for 10% of the reflections excluded from all refinement and were chosen in thin resolution shells due to noncrystallographic symmetry.

replacement and refined to an R and R_{free} of 19.5% and 26.1%, respectively. The 2.2 Å structure of the same fragment of EDA-A2 was also determined and refined to an R and R_{free} of 20.0% and 24.1% (Table 1). In both isoforms, the EDA trimer resembles other TNFL family members and is formed by three jelly-roll β sandwich monomers. Each monomer is composed of two sheets containing strands A′AHCF and B′BGDE. Systematically shorter and generally well-ordered CD, EF, and DE loops as well as the long but compactly folded AA′ loop make the EDA trimer more globular and compact than other, more pyramid-shaped TNFL family members (Figure 1).

Unlike either Apo2L/TRAIL (Hymowitz et al., 2000), BAFF (Oren et al., 2002), or the structurally related NC1 domain of collagen X (Bogin et al., 2002), EDA shows no evidence of metal binding. The surface of EDA-A1, including the putative receptor binding region along the monomer-monomer interface, is free of significant cavities or crevices. This surface is even flatter and less charged in EDA-A2 (Figure 2). The lack of any substantial surface features in either isoform is consistent with the expected relatively large receptor interaction area with dispersed binding determinants as previously observed for the LT/TNFR1 (Banner et al., 1993) and Apo2L (TRAIL)/DR5 (Hymowitz et al., 1999; Mongkolsapaya et al., 1999; Cha et al., 2000) complexes.

Like BAFF, EDA was expected to contain a disulfide bond linking strands E and F. Surprisingly, the predicted disulfide bond between Cys 332 and Cys 346 is observed in the structure of EDA-A2 but not EDA-A1. The absence of this disulfide bond in EDA-A1 is likely an artifact resulting from protein production in the reducing environment of the cytosol of *E. coli* and subsequent purification and storage at pH 6.5. EDA-A2 was expressed and purified in a similar fashion, but at a pH more favorable for disulfide bond formation. Formation

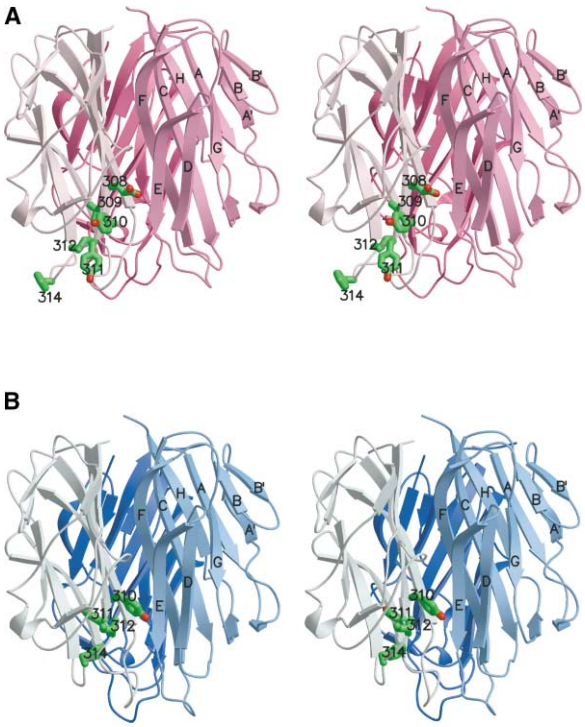

Figure 1. The Crystal Structure of EDA

(A) Walleyed stereo view of a ribbon rendering of the EDA-A1 trimer. The trimer is oriented with its N and C termini at the top of the page. Individual monomers are colored in shades of pink. β strands and relevant amino acids are labeled.

(B) Walleyed stereo view of the EDA-A2 trimer labeled as in (A). Individual monomers are colored in shades of blue.

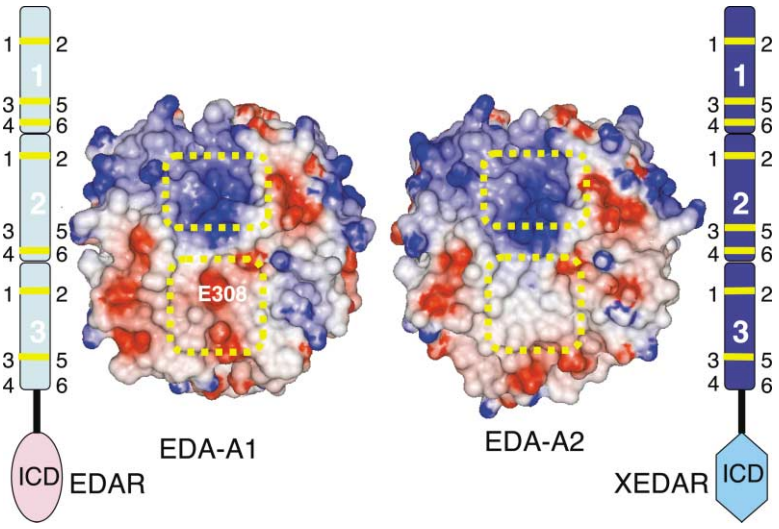

Figure 2. Electrostatic Surface of EDA-A1 (Left) and EDA-A2 (Right) and the Predicted Receptor Binding Site

The molecular surface of both EDA isoforms is colored according to the calculated electrostatic surface potential with +5 kT in blue, neutral in white, and –5 kT in red. The predicted receptor binding surface is outlined in yellow. The subdomain structure of XEDAR and EDAR is depicted schematically with the relative location and number of disulfide bonds indicated by yellow lines. The N termini of the receptors are at the top of the figure. CRDs are labeled.

of this bond is expected in native EDA-A1 material and would only involve repositioning of the sulfur atom of Cys 346 to the corresponding position in EDA-A2 without any further changes to the structure.

Dimers of Trimers in the Asymmetric Units of EDA-A1 and EDA-A2

The crystallographic asymmetric unit of both the EDA-A1 and EDA-A2 crystals contains more than one copy of the biologically relevant trimer. There are four trimers comprised of a total of 12 protomers in the EDA-A1 asymmetric unit and two trimers or six protomers in the EDA-A2 asymmetric unit. This extensive noncrystallographic symmetry provides additional packing-independent information about the EDA structure. The 12 copies of the EDA-A1 protomer have an average root mean square deviation (rmsd) of 0.34 Å from the mean coordinates using Cα atoms for residues 248–388. The only significant variation among the 12 protomers occurs at the beginning of the AA′ loop and at the tips of the CD and EF loops. The most striking difference is the conformation of strand A′ in monomer J, which differs significantly from that of the other monomers, likely due to crystal packing. The asymmetric unit of EDA-A2 shows a greater degree of conformational variability, as reflected by a higher rmsd of 0.80 Å from the mean coordinates using Cα atoms of residues 248 to 389. In particular, the AA′ and EF loops show more divergence than in the EDA-A1 structure. However, in the area of the receptor specificity switch, all copies of both EDA-A1 and EDA-A2 agree well within each isoform but differ considerably between isoforms.

Even though the EDA-A1 asymmetric unit contains four trimers while the EDA-A2 asymmetric unit is composed of two trimers, the crystal packing within the unit cells is similar. The similarity of the crystal packing is due to in part to the presence of an almost identical "dimer of trimers" in the asymmetric unit of both crystals. In both cases, the trimers are oriented parallel to one another such that their termini are on the same side. The interface between the trimers is formed by one monomer-monomer interface from each trimer and buries approximately 2000 Å^2. In this assembly, two of the expected receptor binding sites are obscured, leaving four available. In the EDA-A1 crystals, two pairs of these intimately associated trimers form the four-trimer asymmetric unit, while in EDA-A2 one pair forms the asymmetric unit. Despite the large interface, these dimers of trimers do not associate with high affinity in the absence of the collagen-repeat region; size exclusion chromatography of the TNF domain alone of both EDA-A1 and EDA-A2 indicates that both proteins exist as trimers at 0.2 mM (data not shown). Other than this dimer of trimers, the remaining crystal packing contacts are not unusual and show no indication of formation of higher order assemblies such as those seen in some of the BAFF crystal forms (Liu et al., 2002, 2003; Kim et al., 2003).

Nevertheless, for full activity, soluble EDA trimers need to be oligomerized into higher-order assemblies via the collagen-like region in the EDA stalk. Mutations in this region reduce EDA activity (Bayés et al., 1998; Schneider et al., 2001). It is not known if the collagen-like regions are solely responsible for the oligomerization or if the TNF domains of EDA also interact. Ligation of trimers into higher-order assemblies may increase receptor affinity by avidity, may change the geometry of the ligand-receptor complex, or may be required in order to recruit adaptor proteins to the intracellular domains of the receptors. While constructs of EDA-A1 and EDA-A2 lacking the collagen-like region pack in the crystals as dimers of trimers, the physiological importance, if any, of this interface is unclear.

The Structure of the EDA-A1 Receptor Specificity Switch

In EDA-A1, the receptor specificity switch (residues Glu 308 and Val 309) forms the C-terminal portion of strand C and is followed by a β bulge created by residues Tyr 310 and Tyr 311, which in turn are connected to a six-residue loop that leads to strand D. Glu 308 and Val 309 are part of a β strand (Figures 1A and 3A) and make many interactions with the adjacent GH loop and strand F. In particular, the side chain conformation of Glu 308

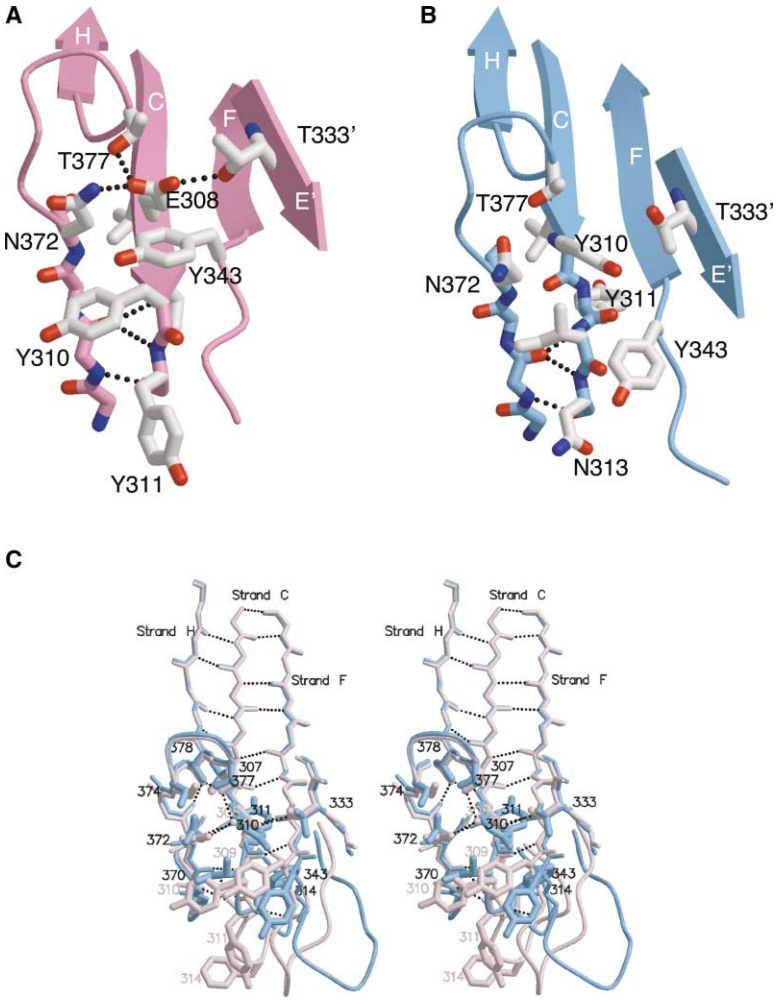

Figure 3. Details of the Receptor Specificity Switch

(A) EDA-A1 Glu 308 is tightly positioned. Residues surrounding Glu 308 are shown. The β strands formed by the backbone are represented as arrows. Side chains have been omitted from most residues for clarity. Hydrogen bonds are indicated by dashed lines.

(B) EDA-A2 residues surrounding Tyr 310.

(C) Walleyed stereo view of a superposition of the specificity switch regions of EDA-A1 (pink) and EDA-A2 (blue). Selected EDA-A2 residues are labeled in black. Where the EDA-A1 and EDA-A2 structures differ considerably, EDA-A1 residues are labeled in pink.

is reinforced by hydrogen bonds to Thr 333 in strand E of the neighboring monomer as well as to Asn 372 and Thr 377 in the adjacent GH loop. Val 309 packs in the hydrophobic core of the monomer. The next two residues, Tyr 310 and Tyr 311, form an antiparallel classical β bulge (Chan et al., 1993) with Ser 370, which is part of a partial strand in the GH loop. These two residues are followed by irregular extended structure until residue Phe 314, where a turn from Phe 314 to Phe 317 connects to strand D. This turn is well ordered in some copies and poorly ordered in others and is a site of deviation from the noncrystallographic symmetry. Asn 313 is glycosylated when EDA is expressed in mammalian cells (Schneider et al., 2001). This residue is at the tip of the CD loop, and the glycosyl-modified side chain is not likely to significantly influence either receptor binding or ligand structure.

Contrary to assumptions based on sequence analysis and construction of a homology model of EDA-A1 (Yan et al., 2000), Glu 308 and Val 309 do not insert into strand C by forming a β bulge. The inadequacy of the homology model derives mostly from incorrect assumptions about the sequence alignment. In particular, Tyr 310 and Tyr 311 were expected to align with hydrophobic residues at the end of the C strand as seen in Apo2L (TRAIL), TNF, and LT. This observation led to the prediction that Glu 308 and Val 309 would be accommodated as a two-amino acid β bulge. In contrast, the experimental structure shows that Glu 308 and Val 309 are an integral part of the C strand forming regular antiparallel β sheet hydrogen bonding, while Tyr 310 and Tyr 311 form a classical antiparallel β bulge (Figures 1 and 3A).

Receptor Specificity Switch in EDA-A2

In EDA-A2, the C strand is the same length as in EDA-A1, but due to alternative splicing of the mRNA, different residues compose the C-terminal end of this strand. The main chain atoms of Tyr 310 and Tyr 311 occupy the same spatial position as those of Glu 308 and Val 309 in EDA-A1. However, the side chain of Tyr 310 makes very different interactions than are seen for Glu 308. In particular, it does not form any of the hydrogen bonds seen in the EDA-A1 structure. Concomitantly, the side chains of Thr 333 and Tyr 343 are in a different position than in EDA-A1. However, the conformation of the GH loop is essentially identical in both isoforms (Figures 1 and 3).

In the structure of EDA-A2, the β bulge following the C strand is also intact but involves different residues than in EDA-A1 and is formed by Ile 312, Asn 313, and

Ser 370 in all six copies of the EDA-A2 protomer. Both the main chain and side chain conformation of the CD loop differ considerably between the two isoforms. In EDA-A2, Ile 312 is exposed at the surface of the expected receptor binding site and the side chain of Phe 314 is completely buried, while in EDA-A1, Ile 312 is buried and Phe 314 is exposed. The CD loop is also two residues shorter, which is accommodated by the movement of residues 314 and 315 (Figures 1 and 3). Propagation of insertions or deletions in secondary structure to subsequent loops is not unprecedented and has been seen in the T4 lysozyme model system, where addition of several residues to a helix resulted in reregistering of the helix and lengthening of the following loop rather than an interruption of the helix (Heinz et al., 1993). In EDA, the conformational adaptability of the CD loop between isoforms is not surprising, as this loop does not seem to be well packed in the EDA-A1 structure as reflected by higher temperature factors and greater NCS deviations than in the rest of the ligand. Altered packing of the CD loop in EDA-A2 causes a shift of the main chain of the EF loop by up to 6 Å, although the conformation of this loop is generally similar to that seen in the EDA-A1 structure.

Differences between EDA-A1 and EDA-A2 in the Expected Receptor Binding Site

EDA-A2 differs from EDA-A1 only by the absence of Glu 308 and Val 309. This variation causes considerable alteration to the surface of the protein due to different chemical properties, shape, and orientation of the side chains at the expected receptor binding site. In particular, the differences in both shape and chemical characteristics between the Glu (EDA-A1) and Tyr (EDA-A2) moieties have two significant effects. First, loss of the negative charge drastically changes the electrostatic characteristics of the ligand surface. EDA-A1 has a region of negative surface charge at the center of the expected receptor binding site, while the surface of EDA-A2 is largely neutral in this area (Figure 2). Second, the receptor binding surface is even flatter and more featureless in EDA-A2 than in EDA-A1 due to rearrangement of the residues forming the binding site, including the reorientation of Tyr 343, and the presence of Tyr 310 and Ile 312 at the center of the site (Figure 3). The altered positions of these amino acids result in differences in the surface characteristics between EDA-A1 and EDA-A2 that are sufficient to determine receptor specificity.

Receptor Chimeras Indicate that CRD3 Determines Specificity

In order to determine which portions of the receptors are responsible for ligand specificity, several chimeras between EDAR and XEDAR were made and assayed for binding with limited success (Figure 4). Chimeras in which either CRD1 alone or both CRD1 and CRD2 of XEDAR were replaced with the corresponding domains from EDAR retained specificity for EDA-A2. These data indicate that CRD1 and CRD2 of XEDAR are not required for discrimination between EDA-A1 and EDA-A2. Instead, these experiments indicate that ligand specificity

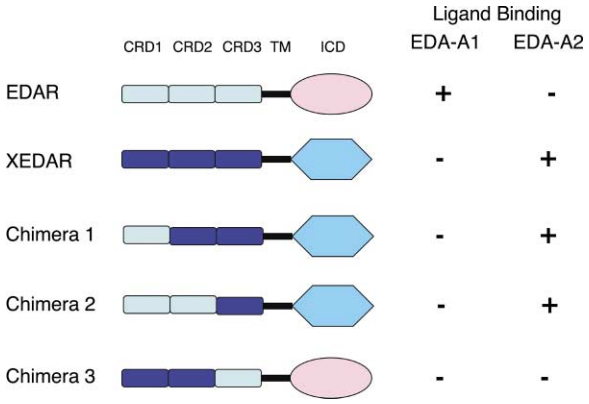

Figure 4. Functional Redundancy of CRD1 and CRD2 of EDAR and XEDAR

Schematic depiction of the receptor chimeras and their observed ligand specificity.

determinants reside in CRD3 of XEDAR. By analogy, CRD3 of EDAR is expected to be required for recognition of EDA-A1. The reverse chimera composed of CRD1 and CRD2 of XEDAR with CRD3 of EDAR did not bind either EDA-A1 or EDA-A2, suggesting that CRD3 from EDAR is not structurally compatible with CRD1 and CRD2 from XEDAR. This incompatibility prevents experimental confirmation of the EDAR binding determinants for EDA-A1.

These data are also consistent with the structures of LT with TNFR1 and Apo2L (TRAIL) with DR5, in which CRD3 of the receptors contacts the ligand surface in the region corresponding to the EDA specificity switch. In contrast, the surfaces of EDA with which CRD2 is predicted to interact are essentially the same in both isoforms (Figure 2). Thus, any contacts made by CRD2 from EDAR and XEDAR with the ligand should be functionally redundant; i.e., the specificity of a receptor hybrid will correlate with the identity of CRD3 as shown by the chimera data.

In order to further understand the receptor specificity switch, homology models of EDAR and XEDAR were made using the structure of TNFR1 as a template. The models of the receptors were docked onto the structures of EDA-A1 and EDA-A2, and are in agreement with the chimera data as they also indicate that CRD3 interacts with the receptor specificity switch. The low level of sequence identity between either EDAR or XEDAR to TNFR1 as well as the lack of regular secondary structure and the nonglobular fold of the TNF receptors severely limits the accuracy of these homology models and prevents more detailed analysis of receptor-ligand interactions. Determination of cocrystal structures of either EDA-A1 with EDAR or EDA-A2 with XEDAR will be required for elucidation of the atomic details of the specificity determinants of the receptors.

Location of Mutations That Cause HED

Mutations in EDA, EDAR, and EDARDD can cause HED (Monreal et al., 1998; Tucker et al., 2000; Schneider et al., 2001; Headon et al., 2001; Yan et al., 2002). While many of the alterations affecting EDA involve either

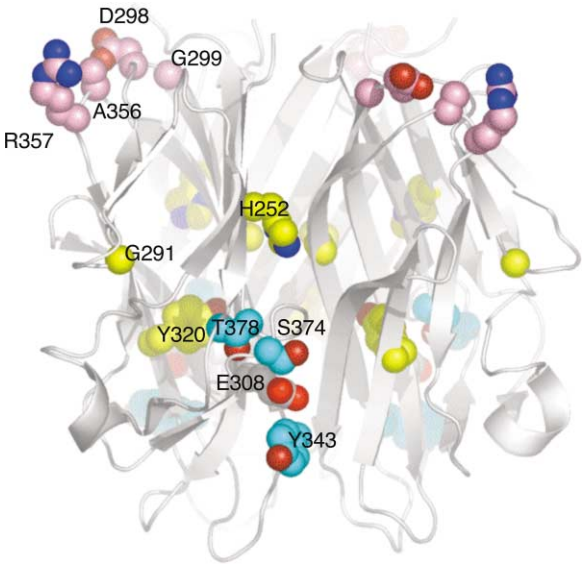

Figure 5. Locations of HED Mutations

The EDA-A1 trimer is shown as a ribbon rendering in white with relevant side chains rendered in spheres. The carbon atoms of mutations likely to affect overall ligand structure are colored yellow, mutations near Glu 308 are colored cyan, and mutations forming a distinct surface patch are colored pink.

frameshifts or gene truncations with concomitant alterations in, or the absolute absence of, the EDA message, missense mutations have also been described which result in a single point mutation in the EDA protein. Many of these mutations have recently been cataloged and mapped to the appropriate domains of the mature protein (Schneider et al., 2001). Determination of the structure of the TNFL domain of EDA permits dissection of the molecular details of the mutations affecting this domain (Figure 5).

The HED-causing mutations that affect the TNFL domain of EDA can be divided into three classes: mutations which likely affect the overall structure of EDA, mutations which affect the receptor binding site, and mutations whose effect is uncertain but which may define a novel interaction site. In the first group, the individual mutations His252Leu, Gly291Trp, Gly291Arg, Gly299Ser, Tyr320Cys, or Ala349Asp probably globally destabilize the ligand (Figure 5). All of these mutations either replace small amino acids with larger residues that cannot be accommodated structurally, or replace large amino acids in the core of the protein with residues that cannot make the same packing interactions.

In the second class, the HED-causing point mutations Tyr343Cys, Ser374Arg, Thr378Pro, or Thr378Met are all located adjacent to the receptor specificity switch and are predicted, based on the structures presented here, to either form (Tyr 343, Ser 374) or buttress (Thr 378) parts of the receptor binding site. The mutation of Tyr 343 to Cys is of particular interest, since this residue is in a different conformation in the EDA-A1 and A2 structures. Furthermore, recombinant EDA-A1 containing this mutation is trimeric and soluble, but does not bind EDAR (Schneider et al., 2001). Two of these residues, Tyr 343 and Ser 374, are also buried in the interface formed by the dimer of trimers in the crystallographic asymmetric unit.

In the final group, the seemingly innocuous point mutations of Asp298His, Ala356Asp, and Arg357Pro, as well as the variant Gly299Ser, are clustered together at the surface of the protein, suggesting that they might form an additional binding site (Figure 5). However, since this area of the ligand surface is not expected to form part of the canonical receptor binding site, nor is it involved in the crystal packing contact forming the dimer of trimers, the function of this site is unknown. It is also possible that some of these mutations may deleteriously affect the ligand by altering its solution or folding properties. This is supported by the observation that recombinant EDA-A1 and A2 carrying the Ala356Asp mutation are not properly secreted by mammalian cells (Schneider et al., 2001).

Conclusions

Proteins evolve and achieve specificity in diverse ways. The relationship between EDA-A1 and EDA-A2 is an elegant example of evolution at work. Two almost identical proteins, whose differences are due to alternative splicing of the same gene, interact specifically with two very divergent receptors. The two amino acid difference between EDA-A1 and EDA-A2 has considerable effects on the electrostatics and shape of the protein surfaces in the vicinity of the receptor binding site. These differences determine receptor specificity and form the basis of a receptor specificity switch. The structures of the EDA-A1 and EDA-A2 isoforms, the effects of naturally occurring, disease-causing mutations in the TNF domain, and characterization of chimeric receptors all support this conclusion. The disparity in conservation between EDAR and XEDAR versus EDA-A1 and EDA-A2 suggests that the evolutionary histories of the EDA isoforms and their receptors may be very different. The recent discovery of two receptors, TROY and RELT (Eby et al., 2000; Kojima et al., 2000; Sica et al., 2001), with significant homology to EDAR and XEDAR, respectively, but without known ligands, suggests that other ligands, or possibly additional EDA splice variants, might exist which interact with these receptors and could potentially crossreact with EDAR or XEDAR.

Experimental Procedures

Protein Expression, Purification, and Crystallization

A gene optimized for expression of EDA-A1 in *E. coli* was purchased from Aptagen, Inc. (Herndon, VA), in order to overcome the very low expression levels found in *E. coli* for the natural human sequence. DNA encoding EDA-A1 residues 233–391 was subcloned into the pET15b vector and then transformed into BL-21 (DE3) cells carrying pLysS. Cells were grown at 37°C until mid-log phase in LB medium with 50 mg/ml carbenicillin, then cooled to 16°C prior to induction with 1 mM IPTG. 50 g of fermentation cell paste was resuspended in 50 mM Tris (pH 8), 500 mM NaCl, and 10 mM imidazole and lysed by passage through a microfluidizer. The soluble fraction was loaded onto a Ni-NTA agarose column and eluted with a step gradient of 275 mM imidazole. The EDA-A1-containing fractions were pooled, 1 unit of thrombin was added per mg of fusion protein, and the solution was dialyzed overnight at 4°C against 20 mM Tris (pH 7) and 1 mM $CaCl_2$. The dialysate was loaded on a monoS column pre-equilibrated in 20 mM Bis-Tris (pH 6.5); EDA-A1 was eluted with

a 0 to 1 M NaCl gradient. The fractions containing EDA-A1 were further purified on a S-200 size exclusion column equilibrated in 20 mM Bis-Tris (pH 6.5) and 200 mM NaCl. Fractions corresponding to trimeric protein were pooled. Final yield was 15 mg purified protein per 50 g of cell paste.

The purified protein was concentrated to 8.5 mg/ml and used for crystallization trials. After several weeks at 19°C, EDA-A1 crystallized as thin plates in 4 μl hanging drops consisting of 2 μl protein and 2 μl well solution over a well solution of 20% PEG 3350 and 0.2 M di-sodium hydrogen phosphate. The crystals were immersed in a solution of 18% PEG 3350, 0.16 M di-sodium hydrogen phosphate, and 20% PEG 300 prior to cryocooling by immersion in liquid nitrogen.

DNA encoding EDA-A2 residues 233–391 was generated via PCR using the optimized EDA-A1 gene as a template and oligonucleotide primers containing the deletion of the sequence encoding residues Glu 308 and Val 309. This construct was subcloned into the pET15b vector and expressed in BL21 (DE3) cells as described for EDA-A1. 50 g of EDA-A2 fermentation cell paste was microfluidized in 50 mM Tris (pH 8), 500 mM NaCl and 10 mM imidazole. The lysate was separated by centrifugation and the supernatant loaded onto a Ni-NTA agarose column. The column was washed with 20 mM imidazole and the protein eluted with eight column volumes of 250 mM imidazole buffer. Fractions containing EDA-A2 were pooled, thrombin was added, and the solution was dialyzed at 4°C overnight against 20 mM Tris (pH 7.5) and 200 mM NaCl. Dialyzed protein was then concentrated and further purified on a S-200 size exclusion chromatography column. Final yield of trimeric EDA-A2 was 27 mg of protein from 50 g of cell paste.

Purified EDA-A2 was concentrated to 12 mg/ml and used in the Hampton Research high-throughput index screen. Crystals formed after one month at 19°C in 2 μl drops consisting of 1 μl protein solution and 1 μl well solution containing 25% PEG 3350, 0.2 M NaCl, and 0.1 M HEPES (pH 7.5). The EDA-A2 crystals were immersed in 20% PEG 3350, 0.16 M NaCl, 0.08 M HEPES (pH 7.5), and 20% PEG 300 prior to cryocooling.

Data Collection, Structure Solution, and Model Building

A 2.3 Å data set for EDA-A1 was collected at SSRL beamline 7-1. A 2.23 Å data set for EDA-A2 was collected in-house using a Rigaku rotating anode X-ray generator and a Mar345 detector (Table 1). The EDA-A1 data were processed with HKL (Otwinowski and Minor, 1997), while the EDA-A2 data were processed with XDS (Kabsch, 1993). Subsequent data manipulation was performed using the CCP4 suite of programs (CCP4, 1994). Data processing statistics indicated that both the EDA-A1 and EDA-A2 crystals belong to space group $P2_1$ rather than to higher symmetry space groups. Computation of the Matthews coefficient suggested that the asymmetric unit of EDA-A1 and EDA-A2 contained 4 trimers and 2 trimers, respectively.

The EDA-A1 structure was solved by molecular replacement using a search model consisting of a truncated Apo2L/TRAIL trimer (from PDB file 1d0g [Hymowitz et al., 1999]) with all of the nonidentical side chains trimmed to Cβ. Using the program AMORE and data in the resolution range from 8 to 4 Å, four trimers were located in the asymmetric unit with reasonable packing, an initial R factor of 45.6%, and a correlation coefficient of 0.39 on Fs. The structure of EDA-A2 was solved using the same approach but with a search model based on the refined EDA-A1 trimer where part of the C strand as well as the CD and EF loops were removed. Two trimers were located with an initial R factor of 38.4% and a correlation coefficient of 0.55 on Fs.

After solvent flattening and NCS averaging (with 12-fold averaging for EDA-A1 and 6-fold averaging for EDA-A2) using the CCP4 program dm, interpretable density was clearly visible for loops and side chains not included in the search model. Cycles of manual rebuilding followed by refinement using XPLOR 98.1 (Brünger, 1992), as implemented by Accelrys and REFMAC5 as implemented in CCP4 resulted in the final model. Strict NCS constraints and subsequently restraints were applied at early stages of refinement for both structures but were found to be detrimental to the R_{free} in later stages and were discarded. Model quality was analyzed using PROCHECK (Laskowski et al., 1993). For EDA-A1, 84.6%, 14.6%, 0.8%, and 0.1% of the 1731 ordered residues are in the most favored, additionally allowed, generously allowed, and disallowed regions of the Ramachandran plot, respectively. For EDA-A2, 83.1%, 15.2%, 1.1%, and 0.7% of the 840 ordered residues are in the most favored, additionally allowed, generously allowed, and disallowed regions, respectively.

Secondary structure and bulge assignment was analyzed with PROMOTIF. Figures were prepared with Molscript (Kraulis, 1991), Render 3D (Merrit and Murphy, 1994), and pymol (Delano Computing).

Acknowledgments

We thank S. Leung for fermentation, J. Yin for advice on construct design, S. Ho, R. Kelley, and R. Krishnamurthy for making expression constructs with the human EDA DNA sequence, P. Ellis and the staff of SSRL beamline 7-1 for assistance with data collection, C. Eigenbrot for discussion of space group relationships, N. Skelton for the ensemble rmsd calculations, C. Wiesmann for critical reading of the manuscript, and our colleagues in the mass spectrometry and protein sequencing groups.

Received: May 5, 2003
Revised: August 20, 2003
Accepted: September 3, 2003
Published: December 2, 2003

References

Banner, D.W., D'Arcy, A., Janes, W., Gentz, R., Schoenfeld, H.-J., Broger, C., Loetscher, H., and Lesslauer, W. (1993). Crystal structure of the soluble human 55 kd TNF receptor-human TNFβ complex: implications for TNF receptor activation. Cell *73*, 431–445.

Bayés, M., Hartung, A.J., Ezer, S., Pispa, J., Thesleff, I., Srivastava, A.K., and Kere, J. (1998). The anidrotic ectodermal dysplasia gene (EDA) undergoes alternative splicing and encodes ectodysplasin-A with deletion mutations in collagenous repeats. Hum. Mol. Genet. *7*, 1661–1669.

Bodmer, J.-L., Schneider, P., and Tschopp, J. (2002). The molecular architecture of the TNF superfamily. Trends Biochem. Sci. *27*, 19–26.

Bogin, O., Kvansakul, M., Rom, E., Singer, J., Yayon, A., and Hohenester, E. (2002). Insight into Schmid metaphyseal chrondrodysplasia from the crystal structure of the collagen X NC1 domain trimer. Structure *10*, 165–173.

Brünger, A.T. (1992). X-PLOR Manual, Version 3.1 (New Haven, Connecticut: Yale University Press).

CCP4 (Collaborative Computational Project 4) (1994). The CCP4 suite: programs for protein crystallography. Acta Cryst. D *50*, 760–763.

Cha, S.-S., Sung, B.-J., Kim, Y.-A., Song, Y.-L., Kim, H.-J., Kim, S., Lee, M.-S., and Oh, B.-H. (2000). Crystal structure of TRAIL-DR5 complex identifies a critical role of the unique frame insertion in conferring recognition specificity. J. Biol. Chem. *275*, 31171–31177.

Chan, A.W.E., Hutchinson, E.G., Harris, D., and Thornton, J.M. (1993). Identification, classification, and analysis of beta-bulges in proteins. Protein Sci. *2*, 1574–1590.

Eby, M.T., Jasmin, A., Kumar, A., Sharma, K., and Chaudhary, P.M. (2000). TAJ, a novel member of the tumor necrosis factor receptor family, activates the c-jun n-terminal kinase pathway and mediates caspase-independent cell death. J. Biol. Chem. *275*, 15336–15342.

Headon, D.J., Emmal, S.A., Ferguson, B.M., Tucker, A.S., Justice, M.J., Sharpe, P.T., Zonana, J., and Overbeek, P.A. (2001). Gene defect in ectodermal dysplasia implicates a death domain adapter in development. Nature *414*, 913–916.

Heinz, D.W., Baase, W.A., Dahlquist, F.W., and Matthews, B.W. (1993). How amino-acid insertions are allowed in an α-helix of T4 lysozyme. Nature *361*, 561–564.

Hymowitz, S.G., Christinger, H.W., Fuh, G., Ultsch, M., O'Connell, M., Kelley, R.F., Ashkenazi, A., and de Vos, A.M. (1999). Triggering

cell death: the crystal structure of Apo2L/TRAIL in a complex with Death Receptor 5. Mol. Cell *4*, 563–571.

Hymowitz, S.G., O'Connell, M.P., Ultsch, M.H., Hurst, A., Totpal, K., Askhenazi, A., de Vos, A.M., and Kelley, R.F. (2000). A unique zinc-binding site revealed by a high-resolution x-ray structure of homotrimeric Apo2L/TRAIL. Biochemistry *39*, 633–640.

Kabsch, W. (1993). Automatic processing of rotation diffraction data form crystals of initially unknown symmetry and cell constants. J. Appl. Crystallogr. *26*, 795–800.

Kim, H.M., Yu, K.S., Lee, M.E., Shin, D.R., Kim, Y.S., Paik, S.-G., Yoo, O.J., Lee, H., and Lee, J.-O. (2003). Crystal structure of the BAFF-BAFF-R complex and its implications for receptor activation. Nat. Struct. Biol. *10*, 342–348.

Kojima, T., Morikawa, Y., Copeland, N.G., Gilbert, D.J., Jenkins, N.A., Senba, E., and Kitamura, T. (2000). TROY, a newly identified member of the tumor necrosis factor receptor superfamily, exhibits a homology with edar and is expressed in embryonic skin and hair follicles. J. Biol. Chem. *275*, 20742–20747.

Kraulis, P.J. (1991). MOLSCRIPT: A program to produce both detailed and schematic plots of protein structures. J. Appl. Crystallogr. *24*, 946–950.

Laskowski, R.A., MacArthur, M.W., Moss, D.S., and Thornton, J.M. (1993). Procheck: A program to check the stereochemical quality of protein structures. J. Appl. Crystallogr. *26*, 283–291.

Laurikkala, J., Pispa, J., Jung, H.-S., Nieminen, P., Mikkola, M., Wang, X., Saarialho-Kere, U., Galceran, J., Grosschedl, R., and Thesleff, I. (2002). Regulation of hair follicle development by the TNF signal ectodysplasin and its receptor Edar. Development *129*, 2541–2553.

Liu, Y., Xu, L., Opalka, N., Kappler, J., Shu, H.-B., and Zhang, G. (2002). Crystal structure of sTALL-1 reveals a virus-like assembly of TNF family ligands. Cell *108*, 383–394.

Liu, Y., Hong, X., Kappler, J., Jiang, L., Zhang, R., Xu, L., Pan, C.-H., Martin, W.E., Murphy, R.C., Shu, H.-B., et al. (2003). Ligand-receptor binding revealed by the TNF family member TALL-1. Nature *423*, 49–56.

Locksley, R.M., Killeen, N., and Lenardo, M.J. (2001). The TNF and TNF receptor superfamilies: integrating mammalian biology. Cell *104*, 487–501.

Merrit, E.A., and Murphy, M.E.P. (1994). Raster3D version 2.0, a program for photorealistic molecular graphics. Acta Crystallogr. D Biol. Crystallogr. *50*, 869–873.

Migone, T.-S., Zhang, J., Luo, X., Zhuang, L., Chen, C., Hu, B., Hong, J.S., Perry, J.W., Chen, S.-F., Zhou, J.X.H., et al. (2002). TL1A is a TNF-like ligand for DR3 and TR6/DcR3 and functions as a T cell costimulator. Immunity *16*, 479–492.

Mikkola, M.L., and Thesleff, I. (2003). Ectodysplasin signaling in development. Cytokine Growth Factor Rev. *14*, 211–224.

Mongkolsapaya, J., Grimes, J.M., Chen, N., Xu, X.-N., Stuart, D.I., Jones, E.Y., and Screaton, G.R. (1999). Structure of the TRAIL-DR5 complex reveals mechanisms conferring specificity in apoptotic initiation. Nat. Struct. Biol. *6*, 1048–1053.

Monreal, A.W., Zonana, J., and Ferguson, B. (1998). Identification of a new splice form of the EDA1 gene permits detection of nearly all X-linked hypohidrotic ectodermal dysplasia mutations. Am. J. Hum. Genet. *63*, 380–389.

Naito, A., Yoshida, H., Nishioka, E., Satoh, M., Azuma, S., Yamamoto, T., Nishikawa, S., and Inoue, J. (2002). TRAF6-deficient mice display hypohidrotic ectodermal dysplasia. Proc. Natl. Acad. Sci. USA *99*, 8766–8771.

Oren, D.A., Li, Y., Volovik, Y., Morris, T.S., Dharia, C., Das, K., Galperina, O., Gentz, R., and Arnold, E. (2002). Structural basis of BLyS receptor recognition. Nat. Struct. Biol. *9*, 288–292.

Otwinowski, Z., and Minor, W. (1997). Processing of X-ray diffraction data collected in oscillation mode. Methods Enzymol. *176*, 307–326.

Schneider, P., Street, S.L., Gaide, O., Hertig, S., Tardivel, A., Tschopp, J., Runkel, L., Alevizopoulos, K., Ferguson, B.M., and Zonana, J. (2001). Mutations leading to X-linked hypohidrotic ectodermal dysplasia affect three major functional domains in the tumor necrosis factor family member ectodysplasin-A. J. Biol. Chem. *276*, 18819–18827.

Sica, G.L., Zhu, G., Tamada, K., Liu, D., Ni, J., and Chen, L. (2001). RELT, a new member of the tumor necrosis factor receptor superfamily is selectively expressed in hematopoietic tissues and activates transcription factor NF-κB. Blood *97*, 2702–2707.

Sinha, S.K., Zachariah, S., Quiñones, H.I., Shindo, M., and Chaudhary, P.M. (2002). Role of TRAF-3 and -6 in the activation of the NF-κB and JNK pathways by X-linked ectodermal dysplasia receptor. J. Biol. Chem. *277*, 44953–44961.

Srivastava, A.K., Pispa, J., Hartung, A.J., Du, Y., Ezer, S., Jenks, T., Shimada, T., Pekkanen, M., Mikkola, M.L., Ko, M.S.H., et al. (1997). The tabby phenotype is caused by mutation in a mouse homologue of the *EDA* gene that reveals novel mouse and human exons and encodes a protein (ectodysplasin-A) with collagenous domains. Proc. Natl. Acad. Sci. USA *94*, 13069–13074.

Tucker, A.S., Headon, D.J., Schneider, P., Ferguson, B.M., Overbeek, P., Tschopp, J., and Sharpe, P.T. (2000). Edar/EDA interactions regulate enamel knot formation in tooth morphogenesis. Development *127*, 4691–4700.

Wisniewski, S.A., Kobielak, A., Trzeciak, W.H., and Kobielak, K. (2002). Recent advances in understanding of the molecular basis of anhidrotic ectodermal dysplasia: discovery of a ligand ectodysplasin A and its two receptors. J. Appl. Genet. *43*, 97–107.

Yan, M., Wang, L.-C., Hymowitz, S.G., Schilbach, S., Lee, J., Goddard, A., de Vos, A.M., Gao, W.-Q., and Dixit, V.M. (2000). Two-amino acid molecular switch in an epithelial morphogen that regulates binding to two distinct receptors. Science *290*, 523–527.

Yan, M., Zhang, Z., Brady, J.R., Schilbach, S., Fairbrother, W.J., and Dixit, V.M. (2002). Identification of a novel death domain-containing adaptor molecule for ectodysplasin-A receptor that is mutated in *crinkled* mice. Curr. Biol. *12*, 1–20.

Accession Numbers

Coordinates for the EDA-A1 and EDA-A2 structures have been deposited at the Protein Data Bank and have been assigned PDB codes 1RJ7 and 1RJ8.